



This is a repository copy of *Synthesis and characterisation of the hollandite solid solution $Ba_{1.2-x}Cs_xFe_{2.4-x}Ti_{5.6+x}O_{16}$ for partitioning and conditioning of radiocaesium* .

White Rose Research Online URL for this paper:
<http://eprints.whiterose.ac.uk/128864/>

Version: Accepted Version

Article:

Bailey, D.J., Stennett, M.C., Mason, A.R. et al. (1 more author) (2018) Synthesis and characterisation of the hollandite solid solution $Ba_{1.2-x}Cs_xFe_{2.4-x}Ti_{5.6+x}O_{16}$ for partitioning and conditioning of radiocaesium. *Journal of Nuclear Materials*, 503. pp. 164-170. ISSN 0022-3115

<https://doi.org/10.1016/j.jnucmat.2018.03.005>

Reuse

Items deposited in White Rose Research Online are protected by copyright, with all rights reserved unless indicated otherwise. They may be downloaded and/or printed for private study, or other acts as permitted by national copyright laws. The publisher or other rights holders may allow further reproduction and re-use of the full text version. This is indicated by the licence information on the White Rose Research Online record for the item.

Takedown

If you consider content in White Rose Research Online to be in breach of UK law, please notify us by emailing eprints@whiterose.ac.uk including the URL of the record and the reason for the withdrawal request.



eprints@whiterose.ac.uk
<https://eprints.whiterose.ac.uk/>

Synthesis and characterisation of the hollandite solid solution $\text{Ba}_{1.2-x}\text{Cs}_x\text{Fe}_{2.4-x}\text{Ti}_{5.6+x}\text{O}_{16}$ for partitioning and conditioning of radiocaesium

Daniel J. Bailey¹, Martin C. Stennett¹, Amber R. Mason¹ and Neil C. Hyatt¹

1- Immobilisation Science Laboratory, Department of Materials Science and Engineering, University of Sheffield, United Kingdom

Abstract

The geological disposal of high level radioactive waste requires careful budgeting of the heat load produced by radiogenic decay. Removal of high-heat generating radionuclides, such as ^{137}Cs , reduces the heat load in the repository allowing the remaining high level waste to be packed closer together therefore reducing demand for repository space and the cost of the disposal of the remaining wastes. Hollandites have been proposed as a possible host matrix for the long-term disposal of Cs separated from HLW raffinate. The incorporation of Cs into the hollandite phase is aided by substitution of cations on the B-site of the hollandite structure, including iron. A range of Cs containing iron hollandites were synthesised via an alkoxide-nitrate route and the structural environment of Fe in the resultant material characterised by Mössbauer and X-ray Absorption Near Edge Spectroscopy. The results of spectroscopic analysis found that Fe was present as octahedrally co-ordinated Fe (III) in all cases and acts as an effective charge compensator over a wide solid solution range.

1. Introduction

To improve the thermal budgeting of a future geological disposal facility (GDF) there is interest in the separation of high heat generating radionuclides from high level radioactive wastes (HLW). ^{137}Cs is considered to be a suitable candidate for such a “partition and condition” concept due its short half-life, high fission yield and heat output ($t_{1/2} = 30.17$ years, 6.15 % fission yield, 0.417 Wg^{-1} ^{1,2}). ^{137}Cs can be separated from the wastestream by solvent extraction, however, other Cs isotopes are co-extracted and separation is impractical. These additional isotopes include ^{135}Cs , a long-lived isotope with $t_{1/2} = 2.3$ million years. Consequently, in a partition and condition approach separated Cs must be immobilised in a robust host matrix suitable for a period of decay storage and ultimate disposal. Cs is currently vitrified with the rest of HLW raffinate however, a tailored ceramic offers the potential of a more durable wastefrom with higher Cs waste loading ³.

A proposed host for separated caesium is hollandite, $\text{A}_x\text{B}_y\text{C}_{8-y}\text{O}_{16}$, where $x \leq 2$ ⁴. A site cations are large and either monovalent or divalent (Na^+ , Ag^+ , K^+ , Rb^+ , Tl^+ , Cs^+ , Sr^{2+} , Ba^{2+} , Ra^{2+} , Pb^{2+}). B and C site cations are more varied with the accommodation of di, tri, tetra, and pentavalent cations possible e.g. Mg^{2+} , Al^{3+} , Ti^{4+} , Sb^{5+} ^{4,5}. The structure comprises corner and edge sharing BO_6 and CO_6 octahedra forming tunnels along the c-axis of the structure, A site ions are located within these tunnels and are typically eight-fold coordinated by oxygen preventing free migration along the tunnels ⁶. The radius ratio of A and B site cations dictates the crystal symmetry of the system and when $R_A/R_B > 2.08$ tetragonal symmetry results (I4/m). For systems where $R_A/R_B < 2.08$, the A site is too small for the tunnel and BO_6 octahedra twist to

reduce the volume of the tunnel resulting in the distortion of the unit cell and the reduction of symmetry to a monoclinic system (C2/m)^{7,8}. Barium titanate hollandites are the basis for many wasteform formulations and have previously been synthesised using a range of additional B site cations including Fe³⁺, Al³⁺, Ga³⁺, Zn²⁺, Cr³⁺ and Ni²⁺^{9,10}.

Previous work has synthesised hollandites containing iron and caesium however, the influence of varying Cs content on the local Fe structural environment has not been investigated^{2,9,11-13}. This study was devised to investigate the stability of the structure, in particular Fe charge compensation, with respect to Cs substitution. We present a comprehensive study of the structural environment of Fe in hollandites in the hollandite system Ba_{1.2-x}Cs_xFe_{2.4-x}Ti_{5.6+x}O₁₆ where $0 \leq x \leq 0.6$ as determined by Mössbauer and X-ray absorption spectroscopy measurements.

2. Experimental methods

2.1 Material synthesis

Hollandite precursors were produced via the alkoxide route in 10 g batches. Stoichiometric amounts of Ba, Cs and Fe (III) nitrates were dissolved in warm water (~ 50 mL) and mixed with a solution consisting of equal parts titanium (IV) isopropoxide and isopropanol. The resultant slurry was stir dried on a hot plate to remove the majority of excess water and then dried in an oven at 95 °C. The dried powder cake was broken up by passing through a 250 µm sieve and then calcined at 750 °C for one hour. The calcined material was mixed with isopropanol to form a thick slurry and ball milled for 16 hours in a HDPE vessel with yttria-stabilised zirconia milling media. After milling, the slurries were dried and passed through a 250 µm sieve prior to further processing.

Consolidated hollandites were produced by cold uniaxial pressing and sintering (CUP). Hollandites were uniaxially pressed in a 10 mm hardened steel die with a load of 2 atmospheres and reacted for 4 hours in air at 1,250 °C (ramp rate = 5 °Cmin⁻¹).

2.2 Material characterisation

Reacted pellets were ground into a fine powder and characterised by powder X-ray diffraction (XRD). XRD was performed using a Bruker D2 Phaser diffractometer utilising Cu K α radiation, utilising a Ni foil K β filter and a point step of 0.02 from 10 – 70 ° 2 θ . Lattice parameters were determined by performing Le Bail fitting of XRD data using Bruker TOPAS software.

Sintered pellets were characterised by scanning electron microscopy (SEM) using a Hitachi TM3030 SEM equipped with a Bruker Quantax EDX. An accelerating voltage of 15 kV was used for imaging. Sintered pellets were prepared for SEM analysis by mounting in cold setting resin and polishing with SiC paper and progressively finer diamond pastes to an optical finish (1µm). Open porosity was estimated by image analysis using ImageJ, a threshold was applied to images to delineate pores and the area measured. Polishing was performed using oil-based lubricants to prevent the solvation of any Cs-rich phases in aqueous media. Samples were sputter coated with carbon to reduce surface charging effects.

The composition of synthesised hollandites was determined by energy dispersive X-ray fluorescence spectroscopy using a Panalytical Zetium instrument. Measurements were made on sintered, polished pellets under vacuum using Rh X-rays.

^{57}Fe transmission Mössbauer spectra of powdered samples were acquired at room temperature using a $^{57}\text{Co}/\text{Rh}$ source. Samples were calibrated relative to an $\alpha\text{-Fe}$ foil reference and spectra were measured using a constant acceleration waveform with velocity range $\pm 10 \text{ mm s}^{-1}$. Data were deconvoluted by assigning Lorentzian doublets to represent different Fe oxidation states and co-ordination environments using the Recoil analysis software ¹⁴.

The density of synthesised hollandites was determined by helium gas pycnometry. Sample volume was determined using a Micromeritics Accupyc 1340 II pycnometer and sample mass was measured to an accuracy of $\pm 0.0001 \text{ g}$ prior to measurement.

2.3 X-ray absorption spectroscopy (XAS)

Fe oxidation state and co-ordination environment were determined by Fe K-edge XANES (7112 eV). Samples were measured at Beamline 10 of the Dortmund Electron Accelerator (DELTA), University of Dortmund. Incident (I_0) and transmitted (I_t) X-ray intensities were measured using ion chambers, energy calibration was performed using XANES spectra measured with a reference ion chamber (I_r) of a standard placed after the transmission ion chamber in the beam path. X-ray energies were tuned with a channel cut Si (111) monochromator and spectra were acquired from 7000 – 7500 eV. Data were acquired in transmission mode. Samples were measured alongside standards of well defined oxidation state and co-ordination environment by oxygen: staurolite (Fe(II) – tetrahedral, $\text{Fe}_2\text{Al}_9\text{O}_6(\text{SiO}_4)_4(\text{O},\text{OH})_2$), siderite (Fe(II) – octahedral, FeCO_3), synthetic FePO_4 (Fe(III) – tetrahedral) and aegerine (Fe(III) – octahedral, $\text{NaFeSi}_2\text{O}_6$). Fits to Fe pre-edge data of hollandite samples and standards were performed in the energy range 7104-7119 eV (0.3 eV energy resolution) to reveal oxidation state and co-ordination environment information.

The pre-edge features observed in the XANES spectra were fitted following the method proposed by Wilke et al ¹⁵, such fitting permitting direct comparison with other data gathered in previous studies regarding Fe co-ordination in minerals and glass melts. Data were normalised to a unit edge step using the Athena software package ¹⁶, and the rising edge background was fit using an arctangent function. Gaussian components were then fit to the data to describe the components of the pre-edge features. The height and position of the weighted mean centroids of the functions were taken to be representative of the pre-edge feature.

3. Results and discussion

X-ray powder diffraction showed that the structure adopted by the reacted hollandites was dependant on the level of Cs substitution. For $x \geq 0.1$ the system adopted a tetragonal structure whereas when $x = 0$ a monoclinic structure was observed, see Figure 1 below. The transition from the monoclinic to tetragonal structure between $0.0 < x < 0.1$ is in agreement with data reported by Cheary et al (1986) ¹⁷. The presence of a secondary rutile phase was evident however, attempts to determine the rutile content by Rietveld refinement were unsuccessful.

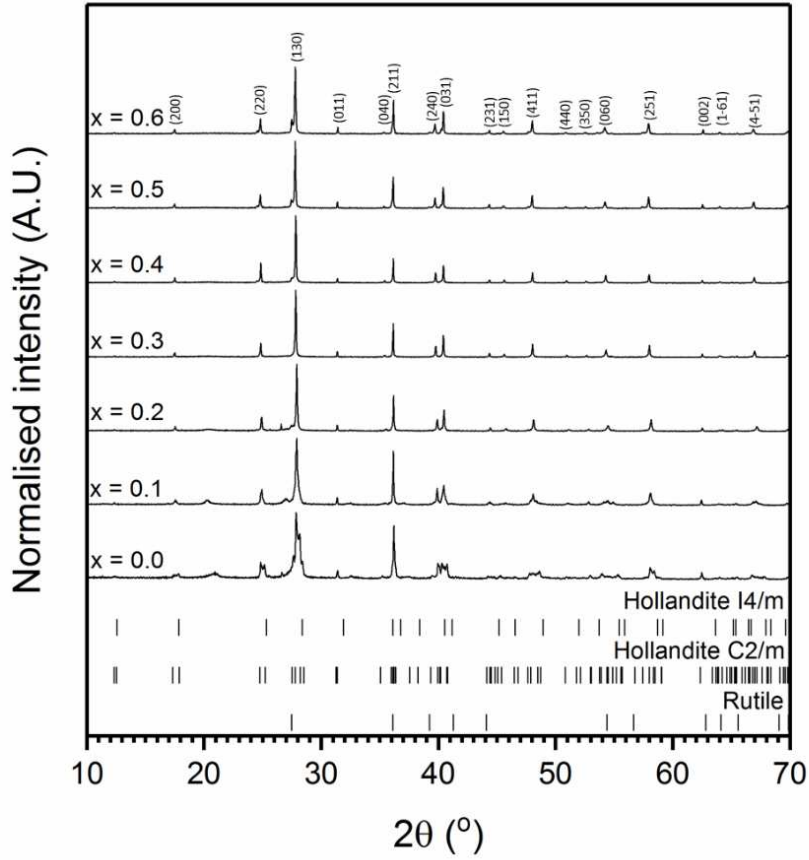


Figure 1: XRD patterns of synthesised Ba-Cs-Fe hollandites. Tick marks show allowed reflections for reference materials. Miller indices refer to the I4/m structure. Reference patterns were obtained from the ICSD database (Hollandite I4/m- ICSD 418150, Hollandite C2/m- ICSD 60792 and Rutile- ICSD 33837).

Diffuse intensity and several satellite peaks were observed in the XRD data for $x = 0.0$ and $x = 0.1$ compositions, these have been reported in previous studies and are attributed to incommensurate ordering of the A-site cations with satellite peaks becoming sharper with increased ordering^{7,18–20}. Unit cell parameters were found by performing a Le Bail fitting of XRD data, the results are given in Table 1.

Table 1: Lattice parameters and density of synthesised hollandites as determined by Le Bail refinement and helium pycnometry.

Nominal composition	r_B (Å)	a (Å)	b (Å)	c (Å)	β (°)	V	ρ ($g \cdot cm^{-3}$)
$Ba_{1.2}Fe_{2.4}Ti_{5.6}O_{16}$	0.6170	10.184(1)	2.9735(3)	9.974(1)	90.789(6)	302.321(6)	4.59 (1)
$Ba_{1.1}Cs_{0.1}Fe_{2.3}Ti_{5.7}O_{16}$	0.6165	10.106(1)	2.9726(2)	-	-	303.592(2)	4.57 (1)
$Ba_{1.0}Cs_{0.2}Fe_{2.2}Ti_{5.8}O_{16}$	0.6160	10.091(1)	2.9681(1)	-	-	302.696(1)	4.54 (1)
$Ba_{0.9}Cs_{0.3}Fe_{2.1}Ti_{5.9}O_{16}$	0.6155	10.128(1)	2.9688(1)	-	-	304.541(1)	4.48 (1)
$Ba_{0.8}Cs_{0.4}Fe_{2.0}Ti_{6.0}O_{16}$	0.6150	10.128(1)	2.9686(1)	-	-	305.297(1)	4.46 (1)
$Ba_{0.7}Cs_{0.5}Fe_{1.9}Ti_{6.1}O_{16}$	0.6145	10.143(1)	2.9680(1)	-	-	305.451(1)	4.49 (5)
$Ba_{0.6}Cs_{0.6}Fe_{1.8}Ti_{6.2}O_{16}$	0.6140	10.144(1)	2.9660(1)	-	-	305.860(1)	4.49 (1)

As can be seen from Table 1, at the monoclinic-tetragonal transformation there is sharp decrease in the unit cell a parameter. With increasing Cs and Ti substitution (for Ba and Fe respectively) there is a general trend of increasing a parameter after an initial decrease resulting from the change in symmetry (see Figure 2). The b lattice parameter shows a general decreasing trend with increasing Cs and Ti substitution. The ionic radii of Cs and Ba in eight-fold coordination are 1.74 and 1.42 Å respectively²¹, therefore the general trend of increasing unit cell volume is indicative of increasing amounts of Cs being incorporated in the structure, see Table 1.

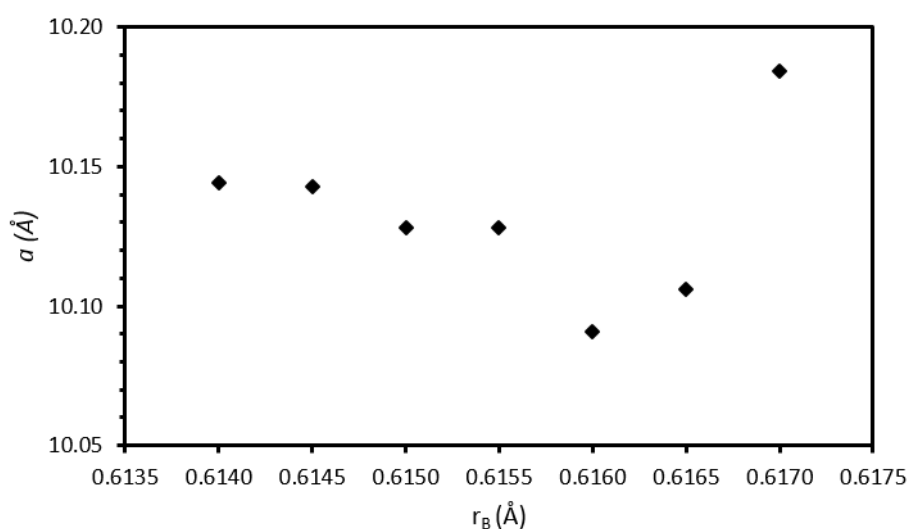


Figure 2: Variation of a lattice parameter with average B-site ionic radius.

Figure 3 shows representative micrographs of the sintered hollandites. As can be seen, hollandite was formed as the majority phase (in agreement with XRD). Secondary rutile was observed throughout the samples often occurring in clusters, see Figure 4. Observed porosity varied from 3 – 12 % with a general increasing trend observed with increasing Cs loading, this indicates that the preparation route could be refined to improve sintering of the materials. Hyatt et al (2006) found that the optimum sintering temperature for Fe-bearing hollandites was 1,330 °C however, these hollandites did not contain Cs and it is likely that increasing the sintering temperature could exacerbate the Cs loss observed (see Figure 5)⁹.

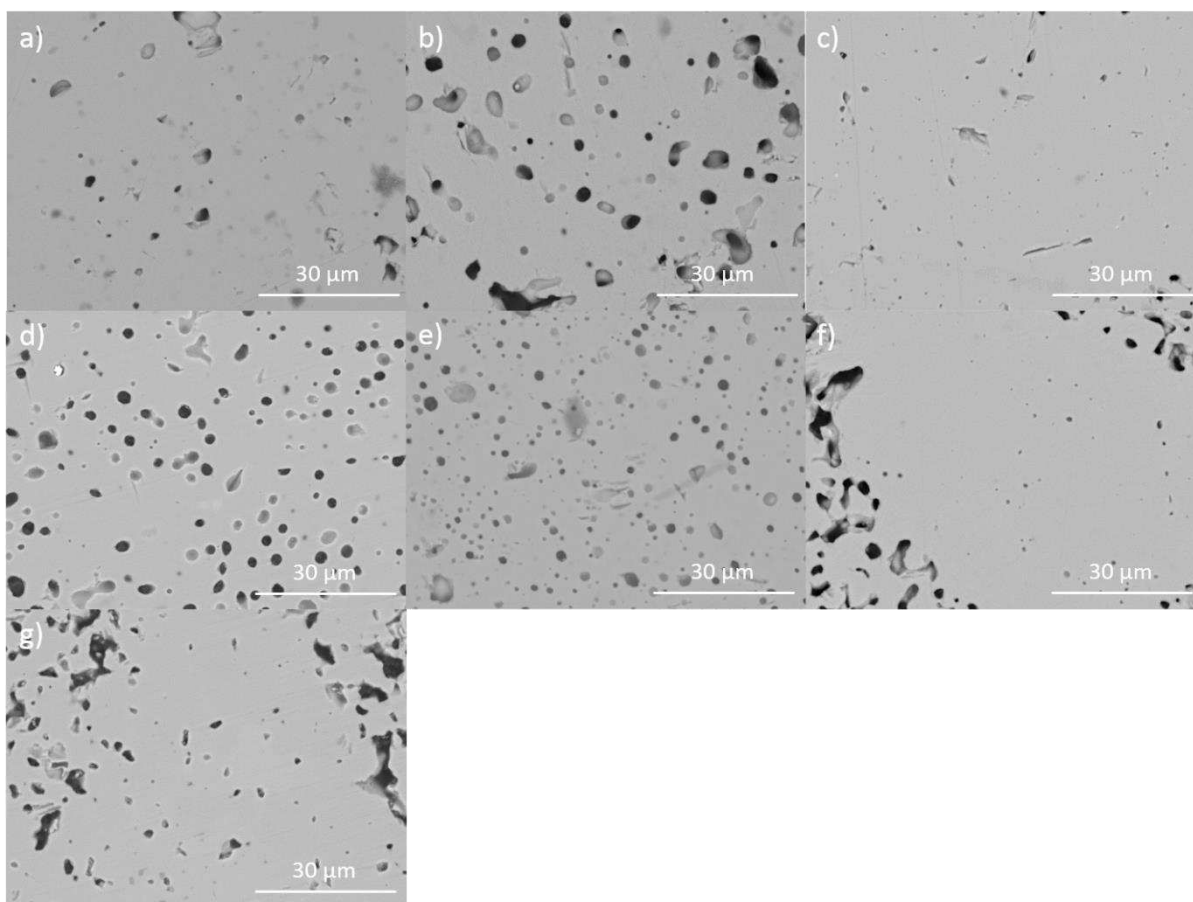


Figure 3: Representative backscattered electron micrographs of “well-sintered” regions of cold uniaxially pressed hollandites, $\text{Ba}_{1.2-x}\text{Cs}_x\text{Fe}_{2.4-x}\text{Ti}_{5.6+x}\text{O}_{16}$: a) $x = 0.0$, b) $x = 0.1$, c) $x = 0.2$, d) $x = 0.3$, e) $x = 0.4$, f) $x = 0.5$ and g) $x = 0.6$.

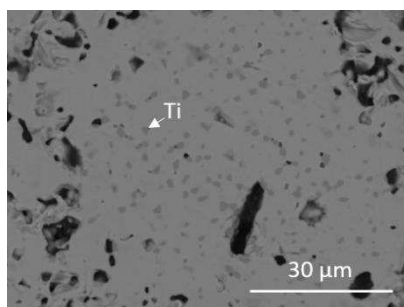


Figure 4: Typical rutile cluster in $\text{Ba}_{0.9}\text{Cs}_{0.3}\text{Fe}_{2.1}\text{Ti}_{5.9}\text{O}_{16}$.

XRF compositional analysis of the synthesised materials found that Cs loss during synthesis was considerable. Retention showed a general increasing trend from $x = 0$ to $x = 0.4$ however, for $x \geq 0.5$ it was found to decrease with increased loading (Figure 5). The marked drop in Cs retention is indicative of reaching the solid solution limit. It is worth noting that XRF analysis is complicated by the presence of secondary rutile in the synthesised hollandites, the relative Ti concentration is artificially inflated by the presence of rutile and suppresses other elements meaning that Cs retention may be higher than observed. The loss of Cs inventory indicates that, although Cs concentration was increased in the samples, the synthesis procedure must be

optimised. A possible method of improving retention of the Cs inventory would be to hot isostatically press samples, the use of a hermetically sealed can prevents Cs volatilisation.

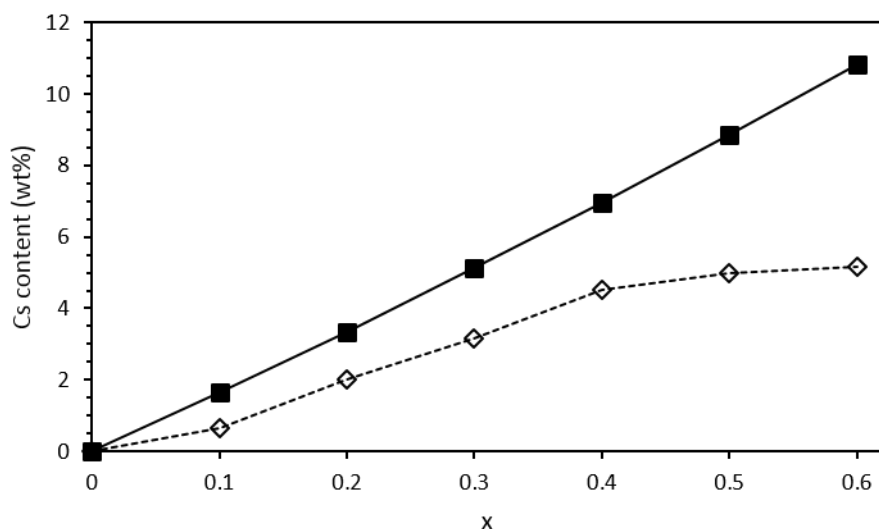


Figure 5: Cs content in synthesised hollandites (wt %): target (black squares) and as determined by XRF (open diamonds).

3.1 Mössbauer spectroscopy

All of the Mössbauer spectra obtained from the samples exhibited one quadrupolar doublet, see Figure 6. It was possible to fit this doublet using one crystallographic site. Fitting a second, octahedrally co-ordinated site was attempted and marginally improved the fit. However, the uncertainty in refined Mössbauer parameters introduced by this (an increase of one order of magnitude) were too great to allow meaningful conclusions to be drawn. Consequently, it was concluded that all Fe occupied a single crystallographic site in the structure. There is a slight asymmetry in the spectra that is not satisfactorily modelled by the addition of a second site and it was therefore concluded that it was as a result of the Goldanskii-Kariagin effect, as observed by Leinekugel-le-Cocq et al, wherein thermal vibrations lead to asymmetry in the absorption spectrum². Extracted Mössbauer fitting parameters were consistent with Fe (III) randomised on one octahedrally co-ordinated site in the solid solution, see Table 2.

Table 2: Mössbauer parameters for $\text{Ba}_{1.2-x}\text{Cs}_x\text{Fe}_{2.4-x}\text{Ti}_{5.6+x}\text{O}_{16}$ hollandites: δ = isomer shift, Δ = quadrupolar splitting and Γ = full width at half maximum.

x	δ (mm.s ⁻¹)	Δ (mm.s ⁻¹)	Γ (mm.s ⁻¹)
0	0.385(1)	0.551(2)	0.180(1)
0.1	0.388(1)	0.541(2)	0.176(2)
0.2	0.380(2)	0.542(3)	0.187(2)
0.3	0.385(2)	0.522(3)	0.172(2)
0.4	0.386(2)	0.517(3)	0.174(2)
0.5	0.388(2)	0.514(3)	0.172(2)
0.6	0.391(2)	0.517(4)	0.176(3)

The hyperfine parameters show variation with Cs substitution similar to the refined lattice parameters. The quadrupolar splitting follows a generally decreasing trend and this implies that the Fe site is becoming progressively less distorted from ideal octahedral symmetry.

The Mössbauer data are in agreement with the results previously reported by Leinekugel-le-Cocq et al. for a hollandite with the composition $\text{Ba}_1\text{Cs}_{0.28}\text{Fe}_{0.82}\text{Al}_{1.46}\text{Ti}_{5.72}\text{O}_{16}$. Leinekugel-le-Cocq et al determined that Fe was present in the Fe (III) oxidation state ². Fe (III) in octahedral co-ordination has also previously been observed in Fe-bearing hollandites by both Birchall et al (1969) for Cs and Cs-Sc containing ferric hollandites ($\text{Cs}_{0.7}\text{Fe}_{0.7}\text{Ti}_{3.3}\text{O}_8$) and by Drofenik and Hanžel (1982) for K containing ferric hollandites ($\text{K}_{1.45}\text{Fe}_{1.45}\text{Ti}_{6.55}\text{O}_{16}$) ^{12,13}. However, our results are somewhat in contrast to those reported by Nguyen et al (2005) who found that Fe^{3+} occupied two distinct sites in ferric Ba-Cs hollandite structures ($\text{Ba}_1\text{Cs}_{0.28}\text{Al}_{1.46}\text{Fe}_{0.82}\text{Ti}_{5.72}\text{O}_{16}$, the most analogous to the compositions studied in this investigation and nominally identical to that studied by Leinekugel-le-Cocq et al) and that irradiation led to the formation of a distinct third site ¹¹. As the tetragonal space group only has one crystallographic site for framework B cations, it is possible to speculate that the pristine samples studied by Nguyen et al were either not single phase or possibly contaminated with other Fe bearing secondary phases. Although there are two Fe sites present in the monoclinic structure, only one quadrupolar doublet is observed for the baseline hollandite composition indicating that Fe is located only on one site in the structure or that, more likely, the two sites are effectively equivalent within the sensitivity of the measurement.

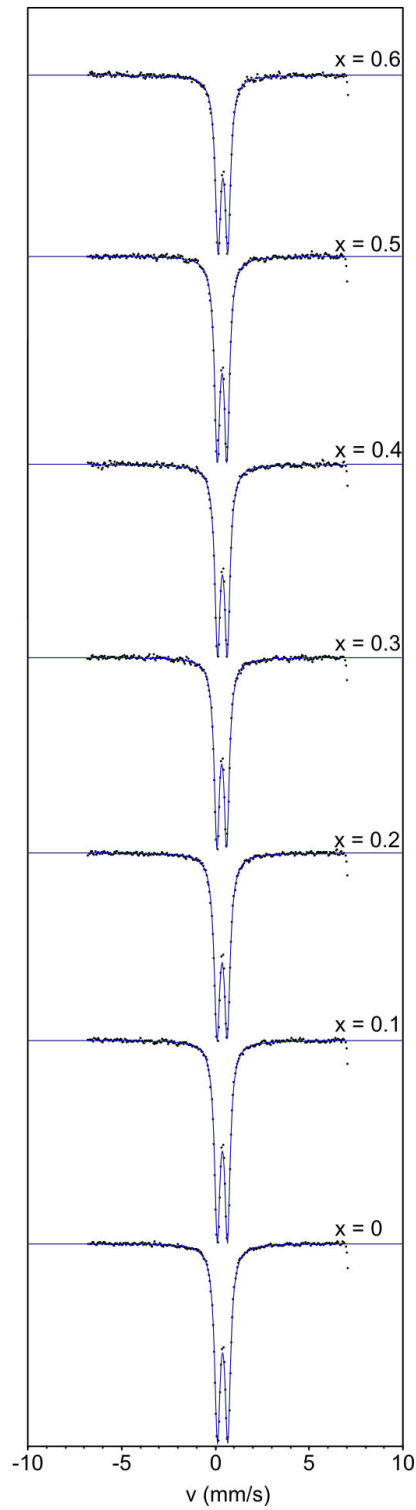


Figure 6: Room temperature Mössbauer spectra of Cs substituted Fe-hollandites $\text{Ba}_{1.2-x}\text{Cs}_x\text{Fe}_{2.4-x}\text{Ti}_{5.6+x}\text{O}_{16}$. Data are shown by black dots, fit is shown by a blue line.

3.2 X-ray absorption spectroscopy

Figure 7a shows the measured XANES spectra of the hollandite samples and standards (FePO_4 , $\text{NaFeSi}_2\text{O}_6$, $\text{Fe}_2\text{Al}_9\text{O}_6(\text{SiO}_4)_4(\text{O},\text{OH})_2$ and FeCO_3). Figure 7b shows a detailed view of the pre-edge region of the XANES spectra in Figure 7a.

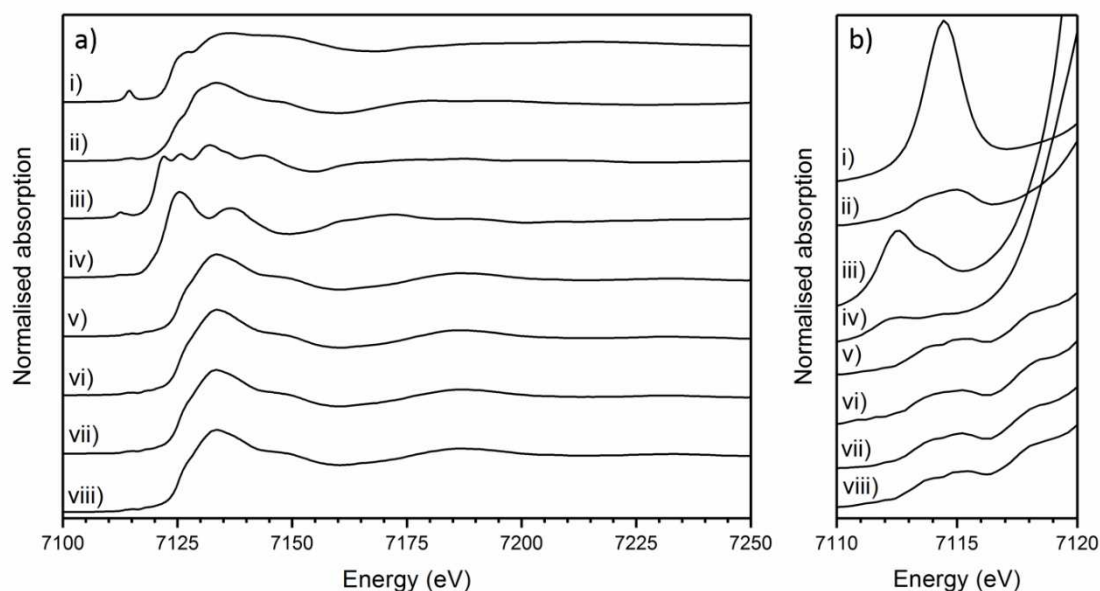


Figure 7: (a) Fe K-edge XANES spectra of hollandite samples and standards; (b) detail of pre-edge XANES features. FePO_4 (i), $\text{NaFeSi}_2\text{O}_6$ (ii), $\text{Fe}_2\text{Al}_9\text{O}_6(\text{SiO}_4)_4(\text{O},\text{OH})_2$ (iii), FeCO_3 (iv), $\text{Ba}_{0.6}\text{Cs}_{0.6}\text{Fe}_{1.8}\text{Ti}_{6.2}\text{O}_{16}$ (v), $\text{Ba}_{0.8}\text{Cs}_{0.4}\text{Fe}_2\text{Ti}_6\text{O}_{16}$ (vi), $\text{BaCs}_{0.2}\text{Fe}_{2.2}\text{Ti}_{5.8}\text{O}_{16}$ (vii), $\text{Ba}_{1.2}\text{Fe}_{2.4}\text{Ti}_{5.6}\text{O}_{16}$ (viii).

Fe K edge XANES data show that the predominant oxidation state of Fe in all hollandite samples is Fe (III). The pre-edge feature is attributed to quadrupolar transitions from bound Fe 1s to 3d states or dipolar transitions from bound 1s to 4p states¹⁵. The 1s to 3d transition is formally forbidden by the dipole selection rule $\Delta l = \pm 1$. This rule is relaxed when Fe is located in a non-centrosymmetric co-ordination environment resulting in 4p-3d mixing and intensified absorption²². Although the weighted mean centroid position and height of the pre-edge feature are related to site symmetry, it has been shown that these features show a linear relationship for average co-ordination number, assuming Fe oxidation state is constant¹⁵. As can be seen there is no significant variation in the pre-edge height or position of this feature for the hollandite samples, as a function of composition and it can therefore be concluded that Fe exists in the same co-ordination environment in all hollandite samples.

The measured XANES spectra were fitted according to the method described by Wilke et al¹⁵. Gaussian functions were fitted to the pre-edge envelope and the height and position of the weighted mean centroids of these functions were taken to represent the overall height and energy of the pre-edge feature. An example fit is shown in Figure 8, fitted values are given in Table 3.

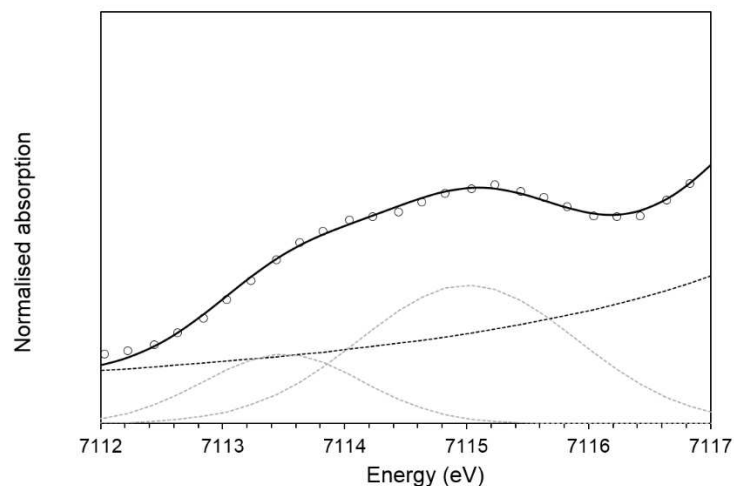


Figure 7: Fitting of XANES features for $\text{BaCs}_{0.2}\text{Fe}_{2.2}\text{Ti}_{5.8}\text{O}_{16}$ sample measured in fluorescence mode. Gaussian (dashed grey lines) and arctangent (dashed black line) functions were used to fit the pre-edge and background features respectively. Data are shown by open symbols, fit is shown by a solid black line.

Table 3: Integrated pre-edge intensity and energies of fitted Fe XANES spectra

Sample	Energy (eV) (± 0.3)	Integrated pre-edge intensity (± 0.03)
$\text{Ba}_{1.2}\text{Fe}_{2.4}\text{Ti}_{5.6}\text{O}_{16}$	7114.5	0.06
$\text{BaCs}_{0.2}\text{Fe}_{2.2}\text{Ti}_{5.8}\text{O}_{16}$	7114.6	0.08
$\text{Ba}_{0.8}\text{Cs}_{0.4}\text{Fe}_2\text{Ti}_6\text{O}_{16}$	7114.4	0.06
$\text{Ba}_{0.6}\text{Cs}_{0.6}\text{Fe}_{1.8}\text{Ti}_{6.2}\text{O}_{16}$	7114.6	0.06
FeCO_3	7112.8	0.07
Staurolite	7112.9	0.19
$\text{NaFeSi}_2\text{O}_6$	7114.3	0.08
FePO_4	7114.3	0.33

Figure 9 shows the correlation of pre-edge height and energy with Fe valence and co-ordination environment of Fe bearing standards (solid diamonds) and synthesised hollandites (open squares). As can be seen the hollandite samples have similar pre-edge heights and energies and lie within the region associated with Fe (III) in octahedral co-ordination (within errors). This is in agreement with the results reported by Hyatt et al (2006) for $\text{Ba}_{1.2}\text{Fe}_{2.4}\text{Ti}_{5.6}\text{O}_{16}$ ⁹.

References

- 1 P. D. Wilson, *The Nuclear Fuel Cycle: From Ore to Waste*, Oxford University Press, Oxford, 1st edn., 1996.
- 2 A. Y. Leinekugel-le-Cocq, P. Deniard, S. Jobic, R. Cerny, F. Bart and H. Emerich, *J. Solid State Chem.*, 2006, **179**, 3196–3208.
- 3 W. E. Lee, M. I. Ojovan, M. C. Stennett and N. C. Hyatt, *Adv. Appl. Ceram.*, 2006, **105**, 3–12.
- 4 A. Byström and A. M. Byström, *Acta Crystallogr.*, 1950, **3**, 146–154.
- 5 A. E. Ringwood, K. D. Reeve, D. M. Levins and E. J. Ramm, in *Radioactive Waste Forms for the Future*, eds. R. C. Ewing and W. Lutze, North Holland Physics Publishing, New York, 1988, pp. 233–335.
- 6 W. Sinclair, G. M. McLaughlin and a. E. Ringwood, *Acta Crystallogr. Sect. B Struct. Crystallogr. Cryst. Chem.*, 1980, **36**, 2913–2918.
- 7 M. L. Carter and R. L. Withers, *J. Solid State Chem.*, 2005, **178**, 1903–1914.
- 8 J. E. Post, R. B. Von Dreele and P. R. Buseck, *Acta Crystallogr. Sect. B Struct. Crystallogr. Cryst. Chem.*, 1982, **38**, 1056–1065.
- 9 N. C. Hyatt, M. C. Stennett, S. G. Fiddy, J. S. Wellings, S. S. Dutton, E. R. Maddrell, A. J. Connelly and W. E. Lee, *Mater. Res. Soc. Symp. Proc.*, 2006, **932**.
- 10 V. Aubin-Chevaldonnet, D. Caurant, a. Dannoux, D. Gourier, T. Charpentier, L. Mazerolles and T. Advocat, *J. Nucl. Mater.*, 2007, **366**, 137–160.
- 11 N. Nguyen, a. Ducouret, F. Studer, V. Aubin, D. Caurant, D. Gourier and J. M. Costantini, *Hyperfine Interact.*, 2005, **166**, 489–493.
- 12 M. Drogenik and D. Hanzel, *Mater. Res. Bull.*, 1982, **17**, 1457–1460.
- 13 T. Birchall, N. N. Greenwood and A. F. Reid, *J. Chem. Soc. A Inorganic, Phys. Theor.*, 1969, 2382.
- 14 D. G. Rancourt and K. Lagarec, "Recoil, Mössbauer Spectral Analysis Software for Windows", 1998.
- 15 M. Wilke, F. Farges, P. E. Petit, G. E. Brown and F. Martin, *Am. Mineral.*, 2001, **86**, 714–730.
- 16 B. Ravel and M. Newville, *Phys. Scr.*, 2005, 1007.
- 17 R. W. Cheary, *Acta Crystallogr. Sect. B Struct. Sci.*, 1986, **42**, 229–236.
- 18 F. C. Mijlhoff, D. J. W. IJdo and H. W. Zandbergen, *Acta Crystallogr. Sect. B Struct. Sci.*, 1985, **41**, 98–101.
- 19 L. A. Bursill and J. Kwiatkowska, *J. Solid State Chem.*, 1984, **52**, 45–52.
- 20 X. J. Wu, F. H. Li and H. Hashimoto, *Acta Crystallogr. Sect. B Struct. Sci.*, 1990, **46**, 111–117.
- 21 R. D. Shannon, *Acta Crystallogr.*, 1976, **32**, 751–767.
- 22 G. A. Waychunas, M. J. Apted and G. E. Brown Jr., *Phys. Chem. Miner.*, 1983, **10**, 1–9.